

## Dissolved Oxygen Balance Model for Neris

Gaudenta Sakalauskienė

*Institute of Mathematics and Informatics  
Akademijos 4, 2600 Vilnius, Lithuania*

Received: 28.03.2001

Accepted: 12.04.2001

### Abstract

We consider a dissolved oxygen balance model for Neris, which includes biochemical oxygen demand, nitrification, sedimentation, algae respiration and photosynthesis. The load from point sources, tributaries and distributed sources are taken into account. Long-term systematic components such as drift and seasonal components are analysed by applying time series analysis.

The model is adapted according to the State Environmental Monitoring, and source data of controlled pollution covering the period 1978-1998.

**Keywords:** water pollution, dissolved oxygen, modelling, time series analysis.

### 1 Introduction

Dissolved oxygen is one of the key parameters when analysing the water quality. Dissolved oxygen depends on the biochemical oxygen demand (deoxygenation), nitrification, reaeration, sedimentation, and photosynthesis and on the algae respiration (Fig. 1). These constituents have six effects on oxygen. First, the biochemical oxygen demand ( $BDS_5$ ) is an equivalent indicator rather than a true physical or chemical substance. It measures the total concentration of dissolved oxygen that would eventually be demanded as wastewater degrades in the river. Second, the conversion of ammonia to nitrate in the nitrification process uses oxygen. Third, the nitrogen can induce plant growth. Fourth, the resulting photosynthesis and respiration of plants can add and delete oxygen from the river. Fifth, the demand of oxygen by sediment and benthic organisms can, in some instances, be a significant fraction of the total

oxygen demand. This is particularly true in small rivers. The sixth effect is the reaeration process. If oxygen is removed from the water column and the concentration falls below the saturation level, there is a tendency to reduce this deficit by the transfer of the gas from the atmosphere through the surface into the stream. If oxygen is added and the water column concentration is greater than the saturation level, the supersaturation is reduced by the transfer of oxygen from the river to the air.

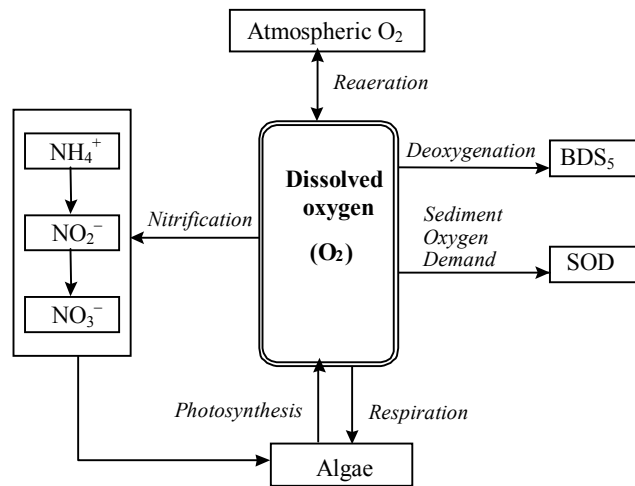


Fig.1. Dissolved oxygen balance.

The mathematical modelling of the river water quality has been and is being dealt with by many authors. In 1925, Streeter and Phelps [1] created a model describing changes in oxygen concentration and its dependence on the organic substances in water (demand of biochemical oxygen). In 1970-1977 the nitrogen transformation impact on oxygen was assessed. The nitrogen transformation rates in water (transformation of ammonia nitrogen into nitrites and nitrates ( $\text{NH}_4^+ \rightarrow \text{NO}_2^- \rightarrow \text{NO}_3^-$ ) were first established by O'Connor and other authors [2, 3]. This transformation was analysed in different rivers [4 and 5]. Stratton, Bridle and others established the nitrification temperature ratio [4]. O'Connor and Di Toro have established the dependence of oxygen concentration in water on photosynthesis and algae [2, 3]. Di Toro [2, 3] established a relationship among the river depth, light energy and amount of algae. The impact of algae on nitrogen transformation was established and described by Thomann, O'Connor and other authors. Thomann and Mueller [6] established the highest algae growth rate within their different populations.

Auer, Canale and Vogel studied the dependence of algae growth on temperature [7, 8].

Daubaras, who studied the demand of biochemical oxygen (BDS<sub>5</sub>) self-purification of the Neris and the Vilnius city sewage disposal effects [9], applied the Streeter-Phelps model. The study of processes related to change in the amounts of organic substances (BDS<sub>5</sub>), to nitrogen transformations in the Nemunas was made by Vincevičienė and Staniškis [10]. The study of biochemical oxygen demand, nitrification, nitrogen transformations and the load from point sources and tributaries in the Neris was analysed by Sakalauskienė [11, 12].

The models of dissolved oxygen described in the literature contain many empirical parameters. Applying a model to a concrete river, these parameters have to be adjusted according to the specific river conditions and the data available. This adjustment for Lithuanian rivers is difficult since the state monitoring measurements are rare (once per month) and asynchronous. Moreover, some important parameters are not measured at all.

In this paper we develop the models described in [11, 12] by modelling the algae impact and more precise modelling of distributed sources. Moreover, applying time series analysis, we estimate the drift, seasonal components of the main processes determining the water quality.

The paper contains four sections. Section 2 presents the mass balance principle and governing equations that form the basis for most water quality models used to simulate the key processes of interest. In the section 3 the model adaptation and some applications to BDS<sub>5</sub>, NH<sub>4</sub><sup>+</sup>, NO<sub>2</sub><sup>-</sup>, NO<sub>3</sub><sup>-</sup> and O<sub>2</sub> is given. Section 4 is devoted to the time series analysis and estimating of drift and seasonal components of the main processes determining the water quality.

The following notation is used throughout the paper:

$c_o(t)$	dissolved oxygen concentration (mgO <sub>2</sub> /l);
$c_{os}(t)$	saturation concentration of dissolved oxygen (mgO <sub>2</sub> /l);
$c_b(t)$	biochemical oxygen demand (mgO <sub>2</sub> /l);
$c_a(t)$	ammonia concentration (mgN/l);
$c_i(t)$	nitrite-nitrogen concentration (mgN/l);
$c_e(t)$	nitrate-nitrogen concentration (mgN/l);
$A(t)$	algae biomass concentration (mgA/l);
$k_o$	reaeration rate coefficient (per day = d <sup>-1</sup> );
$k_b$	demand of biochemical oxygen decomposition rate coefficient (d <sup>-1</sup> );
$k_a$	ammonia oxidation rate coefficient (d <sup>-1</sup> );
$k_i$	nitrite oxidation rate coefficient (d <sup>-1</sup> );
$\mu$	algae growth rate coefficient (d <sup>-1</sup> );
$\rho$	algae respiration rate coefficient (d <sup>-1</sup> );
$K_e$	light extinction coefficient (m <sup>-1</sup> );

$SOD$	temperature-adjusted rate for sediment oxygen demand ( $\text{g/m}^2\text{-d}$ );
$\alpha_1$	oxygen consumed in ammonia oxidation to nitrite ( $\text{mgO/mgN}$ );
$\alpha_2$	oxygen consumed in oxidation of nitrite to nitrate ( $\text{mgO/mgN}$ );
$\beta_1$	oxygen production in photosynthesis per unit of algae biomass ( $\text{mgO/mgA}$ );
$\beta_2$	oxygen uptake in respiration per unit of algae biomass ( $\text{mgO/mgA}$ );
$F(t)$	fraction of algae nitrogen uptake from ammonia pool;
$P_n$	algae preference factor for ammonia;
$T$	temperature ( $^{\circ}\text{C}$ );
$L$	average period (d);
$f$	photoperiod (d);
$I_T$	total daily solar radiation ( $\text{cal cm}^{-2} \text{d}^{-1}$ );
$I_s$	saturation light intensity ( $\text{cal cm}^{-2} \text{d}^{-1}$ );
$K_N$	half saturation constant for nitrogen ( $\text{mgN/l}$ );
$K_P$	half saturation constant for phosphorus ( $\text{mgP/l}$ );
$A_c$	basin area of the reach being loaded ( $\text{m}^2$ );
$v$	flow velocity (m/s);
$Q$	river flow ( $\text{m}^3/\text{s}$ );
$\tilde{Q}$	distributed flow ( $\text{m}^3/\text{s}$ );
$\tilde{c}$	distributed source concentration ( $\text{mg/l}$ );
$H$	average river depth (m);
$t$	travel time (s);
$x$	distance downstream of effluent or monitoring section (m).

## 2 Dissolved Oxygen Balance Model

Dissolved oxygen depends on the biochemical oxygen demand, nitrification process, reaeration, sedimentation and photosynthesis as well as on the algae respiration (see fig. 1).

The full dissolved oxygen balance follows the equation (a first order reaction)

$$\frac{dc_o(t)}{dt} = k_o[c_{os}(t) - c_o(t)] - k_b c_b(t) - \frac{SOD}{H} - k_a \alpha_1 c_a(t) - k_i \alpha_2 c_i(t) + (\beta_1 \mu - \beta_2 \rho) A(t) \quad (2.1)$$

with the initial condition

$$c_o(t_0) = c_{o0},$$

where  $c_o(t)$  and  $c_{os}(t)$  is the dissolved oxygen concentration and its saturation concentration,  $c_b(t)$  is the  $\text{BDS}_5$  concentration,  $c_a(t)$  is the  $\text{NH}_4^+$  concentration,  $c_i(t)$  is the  $\text{NO}_2^-$  concentration,  $A(t)$  is the algae biomass concentration,  $k_o$  is the reaeration rate,  $k_b$  is the  $\text{BDS}_5$  decomposition rate coefficient,  $k_a$  is the  $\text{NH}_4^+$

oxidation rate coefficient,  $k_i$  is the  $\text{NO}_2^-$  oxidation rate coefficient,  $\mu$  is the algae growth rate coefficient,  $\rho$  is the algae respiration rate coefficient,  $SOD$  is the temperature-adjusted rate for SOD,  $H$  is the average river depth,  $\alpha_1$  is the oxygen consumed in ammonia oxidation to nitrite per unit,  $\alpha_2$  is the oxygen consumed in oxidation of nitrite to nitrate per unit,  $\beta_1$  is the oxygen production in photosynthesis per unit of algal biomass and  $\beta_2$  is the oxygen uptake in respiration per unit of algal biomass.

## 2.1 Reaeration

Oxygen saturation concentration decreases with the increase in temperature and salts at normal pressure (APHA 1992):

$$c_{os}(t) = \exp(\varphi(T_a) - 1,81\text{Cl}(t)\psi(T_a)) \quad (2.2)$$

where

$$\varphi(T_a) = -139,34 + \frac{1,57 \times 10^5}{T_a} - \frac{6,64 \times 10^7}{T_a^2} + \frac{1,24 \times 10^{10}}{T_a^3} - \frac{8,62 \times 10^{11}}{T_a^4},$$

$$\psi(T_a) = 1,77 \times 10^{-2} - \frac{1,07 \times 10}{T_a} + \frac{2,14 \times 10^3}{T_a^2},$$

$T_a = T + 273,15$  is the temperature (K) and  $\text{Cl}(t)$  is the chloride concentration (mg/l).

If the water is undersaturated ( $c_o < c_{os}$ ), then the atmospheric oxygen transfers into the water, partially restoring the equilibrium state of saturation. If the water is oversaturated ( $c_o > c_{os}$ ), then this transfer will be inverse.

Many empirical formulas have been suggested for estimating reaeration rate coefficients. Among these, two are commonly used: the O'Connor-Dobbins formula:

$$k_o = k_o(H, T, v) = 3,93v^{0,5}H^{-1,5}(1,047)^{T-20} \quad (2.3)$$

and Churchill's formula

$$k_o = k_o(H, T, v) = 5,026vH^{-1,67}(1,047)^{T-20}. \quad (2.4)$$

Here  $v$  is the average river velocity,  $H$  is the average river depth and  $T$  is the temperature.

The O'Connor-Dobbins and Churchill formulas were developed for different types of streams. Equation (2.3) is applied for ranges of depth  $H = 0,3 \div 9,14$  m and velocity  $v = 0,15 \div 0,49$  m/s and equation (2.4) for ranges  $H = 0,61 \div 3,35$  m and  $v = 0,55 \div 1,52$  m/s.

## 2.2 Biochemical Oxygen Demand

The steady BDS<sub>5</sub> regime in a river is usually described as the first order reaction, i.e.

$$\frac{dc_b(t)}{dt} = -k_b c_b(t) \quad (2.5)$$

with the initial condition

$$c_b(t_0) = c_{b0},$$

where  $c_b(t)$  is the BDS<sub>5</sub> and  $k_b$  is the decomposition rate coefficient.

Literature data have been compiled to correlate  $k_b$  with the stream depth in lieu of any other parameters. The rationale behind this correlation is that the greater the wetted perimeter, the greater the contact with the biological community in the streambed, the most important factor in natural oxidation processes. The tendency for this relation to hold is greater rocky streambeds than for silt beds. However, the general trend appears reasonable up to depths of about 1,5 to 3 m.

To calculate the decomposition rate coefficient, we make use of the formula recommended by Chapros [1]:

$$k_b = k_b(H, T) = 0,3[\min(\frac{H}{2,4}, 1)]^{-0,434} (1,047)^{T-20} \quad (2.6)$$

In other words, for larger and deeper streams (greater than 3 m), the characteristics of the streambed become less of a factor and the level of treatment would distance the following  $k_b$  values: primary – 0,4; intermediate – 0,3; secondary – 0,2 and advanced – 0,1 (d<sup>-1</sup>). That is, for increasing levels of treatment, the residual waste contains a large proportion of refractory organisms and will be less easily oxidised since the treatment processes are designed to oxidise the labile components of the organic matter.

## 2.3 Nitrification

Nitrification follows two stages: the *Nitrosomonas* bacteria transform the ammonia to nitrites, while the *Nitrobacter* bacteria transform nitrites to nitrates (NH<sub>4</sub><sup>+</sup> → NO<sub>2</sub><sup>-</sup> → NO<sub>3</sub><sup>-</sup>), i.e.



The process of nitrification depends on the amount of oxygen, flow rate, suspended solids, concentrations of nitrogen and oxygen, pH and water

temperature (nitrification is most active, when pH  $7 \div 9$ , and the water temperature greater than  $10^\circ\text{C}$ ).

The nitrification process in a river is usually described as the following first order reactions:

$$\begin{aligned}
 \text{Ammonia nitrogen} \quad & \frac{dc_a(t)}{dt} = -k_a c_a(t) - F(t)\alpha\mu A(t), \\
 \text{Nitrite nitrogen} \quad & \frac{dc_i(t)}{dt} = k_a c_a(t) - k_i c_i(t), \\
 \text{Nitrate nitrogen} \quad & \frac{dc_e(t)}{dt} = k_i c_i(t) - (1 - F(t))\alpha\mu A(t),
 \end{aligned} \tag{2.8}$$

with the initial conditions

$$c_a(t_0) = c_{a0}, \quad c_i(t_0) = c_{i0} \quad \text{and} \quad c_e(t_0) = c_{e0}.$$

Here  $c_a(t)$ ,  $c_i(t)$  and  $c_e(t)$  are  $\text{NH}_4^+$ ,  $\text{NO}_2^-$  and  $\text{NO}_3^-$  concentrations, respectively,  $A(t)$  is the algae biomass concentration,  $\alpha$  is the nitrogen fraction of algae biomass,  $\mu$  is the algae growth rate coefficient,

$k_a = k_a(T) = k_{am} 1,085^{T-20}$  is the  $\text{NH}_4^+$  oxidation rate coefficient,

$k_i = k_i(T) = k_{im} 1,058^{T-20}$  is the  $\text{NO}_2^-$  oxidation rate coefficient.

The fraction of algae nitrogen uptake from ammonia pool follow the formula:

$$F(t) = \frac{P_n c_a(t)}{P_n c_a(t) + (1 - P_n) c_e(t)} \tag{2.9}$$

where  $P_n$  is the algae preference factor for ammonia ( $P_n \approx 1$  if  $c_a(t) \neq 0$  and  $P_n \approx 0$  if  $c_e(t) = 0$ ),  $k_{am}$  and  $k_{im}$  are specific oxidation rates at  $20^\circ\text{C}$ .

## 2.4 Photosynthesis and respiration

Through photosynthesis and respiration, *phytoplankton*, *periphyton*, and rooted aquatic plants (*macrophytes*) could significantly affect the dissolved oxygen levels in the water column. The average algae growth rate as a function of light intensity over a given depth of water, is given by Canale and Vogel [5]:

$$\mu = \mu(T, H, I) = 1,8(1,066)^{T-20} \frac{2,718f}{K_e HL} (e^{-\alpha_1} - e^{-\alpha_2}) \min\left(\frac{c_a + c_e}{c_a + c_e + K_N}; \frac{p}{p + K_P}\right), \tag{2.10}$$

$$\alpha_1 = \frac{I_T}{I_s} e^{-K_e H}, \quad \alpha_2 = \frac{I_T}{I_s}$$

where  $L$  is the average period (day),  $f$  is the photoperiod,  $I_T$  is the total daily solar radiation,  $I_s$  is the saturating light intensity,  $K_e = I_s / H$  is the light

extinction coefficient,  $K_N$  and  $K_P$  is the half-saturation constant for nitrogen and phosphorus.

The approximate respiration rate is given by Thomann [2]

$$\rho = \rho(T) = \rho_i (1,08)^{T-20} \quad (2.11)$$

where  $\rho_i$  varies from 0,05 to 0,25. A value of 0,15 is usually used as a first approximation.

## 2.5 Point pollution sources

Applying equation (2.1), we use the standard time-distance change. Suppose that in a river stretch  $[x_0, x]$  there is neither point nor distributed pollution sources. If at time  $t_0$  a water column with an oxygen concentration  $c_{o0}$  were at a river section  $x_0$ , i.e.  $\tilde{c}_o(x_0) = c_o(t_0) = c_{o0}$ , then this water column will reach a river section  $x$  (downstream) at time  $t = t_0 + (x - x_0)/v$  ( $v$  is the average river flow velocity in the stretch  $[x_0, x]$ ), and its oxygen concentration will be  $\tilde{c}_o(x) = c_o(t_0 + (x - x_0)/v) = c_o(t)$ , the solution to equation (2.1) with the initial condition  $c_o(t_0) = c_{o0}$ .

All the tributaries with significant flow (exceeding a certain chosen value  $\epsilon$ ) are regarded as point pollution sources. Calculating the oxygen concentration after a point source, we assume that the river and tributary flows are mixed immediately at the location of tributary, i.e. if a point source is located at a river section  $x$ , then the oxygen concentration after the confluence,  $c_o(x+)$  is given by

$$c_o(x+) = \frac{c_o(x-)Q(x-) + \tilde{c}_o\tilde{Q}}{Q(x-) + \tilde{Q}} \quad (2.12)$$

where  $\tilde{Q}$  and  $\tilde{c}_o$  are the tributary flow and its oxygen concentration, while  $Q(x-)$  and  $c_o(x-)$  are the river flow and its oxygen concentration before the confluence. The same approach is applied to other concentrations.

Hence the point sources are included in the model as the new initial conditions considering river stretches between tributaries.

If there were no effluent discharge from the wastewater treatment plant at the end of first reach, all concentrations calculated at the end of the first reach would have been used as boundary concentrations for the second reach. Because of the wastewater treatment plant discharge at  $x$ , all water quality constituent concentrations have to be calculated assuming a complete mixing of effluent water with stream water and the new values will be used as boundary concentrations to the second reach.

## 2.6 Distributed sources

In order to model the impact of distributed sources, denote the river flow by  $Q(y)$ , the flow velocity by  $v(y)$ , the  $O_2$  (BDS<sub>5</sub>,  $NH_4^+$ ,  $NO_2^-$ ,  $NO_3^-$ ) distributed source concentrations by  $\tilde{c}_o(y)$ ,  $\tilde{c}_b(y)$ ,  $\tilde{c}_a(y)$ ,  $\tilde{c}_i(y)$  and  $\tilde{c}_e(y)$ , respectively. We assume that these functions are continuous and bounded together with the first derivatives.

Consider the river stretch  $[x, x+h]$ , as  $h \rightarrow 0$ . Regarding the dispersed pollution as a point pollution at the section  $x+h$  and using (2.1) and (2.12), we have

$$\begin{aligned} c_o(x+h) = & \left\{ Q(x) + \Delta_h Q(x) \right\}^{-1} \times \left\{ c_o(x) e^{-\varphi(k_o)} Q(x) + c_{os}(x) e^{\varphi(k_o)} Q(x) - \frac{k_b(x)c_b(x)}{k_o(x)-k_b(x)} \left( e^{-\varphi(k_b)} - e^{-\varphi(k_o)} \right) \right\} Q(x) - \\ & - \frac{SOD - (\beta_1\mu - \beta_2\rho)A(x)}{k_o(x)} \left( 1 - e^{-\varphi(k_o)} \right) Q(x) - \frac{k_i(x)c_i(x)\alpha_2}{k_o(x)-k_i(x)} \left( e^{-\varphi(k_i)} - e^{-\varphi(k_o)} \right) Q(x) - \\ & - \frac{k_a(x)\alpha_1 c_a(x)}{k_o(x)-k_a(x)} \left( e^{-\varphi(k_a)} - e^{-\varphi(k_o)} \right) Q(x) + \tilde{c}_o(x) \Delta_h Q(x) \Big\} + o(h), h \rightarrow 0 \end{aligned} \quad (2.13)$$

where  $\Delta_h Q(x) = Q(x+h) - Q(x)$ ,

$$\varphi(k_o) = k_o(x) \frac{h}{v(x)}, \quad \varphi(k_b) = k_b(x) \frac{h}{v(x)}, \quad \varphi(k_i) = k_i(x) \frac{h}{v(x)}, \quad \varphi(k_a) = k_a(x) \frac{h}{v(x)}.$$

In a similar way, using (2.5) and (2.12), we have

$$c_b(x+h) = \left\{ Q(x) + \Delta_h Q(x) \right\}^{-1} \times \left\{ c_b(x) e^{-\varphi(k_b)} Q(x) + \tilde{c}_b(x) \Delta_h Q(x) \right\} + o(h), h \rightarrow 0 \quad (2.14)$$

Furthermore, using (2.8) and (2.12), we get

$$\begin{aligned} c_a(x+h) = & \left\{ Q(x) + \Delta_h Q(x) \right\}^{-1} \times \\ & \times \left\{ c_a(x) e^{-\varphi(k_a)} Q(x) - F(x)\alpha\mu A(x) \frac{1 - e^{-\varphi(k_a)}}{k_a(x)} Q(x) + \tilde{c}_a(x) \Delta_h Q(x) \right\} + o(h), h \rightarrow 0, \end{aligned} \quad (2.15)$$

$$\begin{aligned} c_i(x+h) = & \left\{ Q(x) + \Delta_h Q(x) \right\}^{-1} \times \\ & \times \left\{ c_i(x) e^{-\varphi(k_i)} Q(x) + \frac{k_a(x)c_a(x)}{k_i(x)-k_a(x)} \left( e^{-\varphi(k_a)} - e^{-\varphi(k_i)} \right) Q(x) + \tilde{c}_i(x) \Delta_h Q(x) \right\} + o(h), h \rightarrow 0, \end{aligned}$$

$$\begin{aligned} c_e(x+h) = & \left\{ Q(x) + \Delta_h Q(x) \right\}^{-1} \times \\ & \times \left\{ c_e(x) Q(x) + k_i(x)c_i(x) Q(x) \frac{h}{v(x)} - (1-F(x))\alpha\mu A(x) Q(x) \frac{h}{v(x)} + \tilde{c}_e(x) \Delta_h Q(x) \right\} + o(h), h \rightarrow 0. \end{aligned}$$

Using Taylor' expansion and passing to the limit as  $h \rightarrow 0$ , we obtain the following first-order differential equations:

$$c'_o(x) + c_o(x) \frac{k_o(x)}{v(x)} + [c_o(x) - \tilde{c}_o(x)] \frac{Q'(x)}{Q(x)} + \left( -k_o c_{os}(x) + k_b c_b(x) + \frac{SOD}{H} + k_a \alpha_1 c_a(x) + k_i \alpha_2 c_i(x) - (\beta_1 \mu - \beta_2 \rho) A(x) \right) \frac{1}{v(x)} = 0$$

$$c'_b(x) + c_b(x) \frac{k_b(x)}{v(x)} + [c_b(x) - \tilde{c}_b(x)] \frac{Q'(x)}{Q(x)} = 0,$$

$$c'_a(x) + c_a(x) \frac{k_a(x)}{v(x)} + [c_a(x) - \tilde{c}_a(x)] \frac{Q'(x)}{Q(x)} + F(x) \alpha \mu A(x) \frac{1}{v(x)} = 0,$$

$$c'_i(x) + c_i(x) \frac{k_i(x)}{v(x)} + [c_i(x) - \tilde{c}_i(x)] \frac{Q'(x)}{Q(x)} - \frac{k_a(x) c_a(x)}{v(x)} = 0,$$

$$c'_e(x) + [c_e(x) - \tilde{c}_e(x)] \frac{Q'(x)}{Q(x)} + \left( (1 - F(x)) \alpha \mu A(x) - k_i(x) c_i(x) \right) \frac{1}{v(x)} = 0.$$
(2.16)

The flow may be related to river basins area from which all the point sources are exclude.

Consider the river stretch  $[x_0, x_1]$  where there is no point source loading. We assume that the river flow and the basin area are described by bounded and continuously differentiable functions  $f(y)$  and  $g(y)$ , i.e.

$$Q(x) - Q(x_0) = f(A(x) - A(x_0)),$$

$$A(x) - A(x_0) = g(x - x_0), \quad x \in [x_0, x_1].$$
(2.17)

Then

$$\frac{Q'(x)}{Q(x)} = \frac{f'(A(x) - A(x_0)) g'(x - x_0)}{Q(x_0) + f(A(x) - A(x_0))}.$$
(2.18)

If we assume that  $f$  and  $g$  are linear functions, i.e.

$$f(y) = \beta y, \quad g(y) = \eta y,$$

then

$$\frac{Q'(x)}{Q(x)} = \frac{\beta \eta}{Q(x_0) + \beta(A(x) + \eta(x - x_0))}.$$
(2.19)

Hence, applying a linear approximation to the river stretch  $[x_0, x_1]$ , the coefficients  $\beta$  and  $\eta$  are defined by

$$\beta = \frac{Q(x_1) - Q(x_0)}{A(x_1) - A(x_0)} = \frac{Q(x_1) - Q(x_0)}{\eta(x_1 - x_0)}$$

and

$$\eta = \frac{A(x_1) - A(x_0)}{x_1 - x_0}$$
(2.20)

We assume that the distributed source and the basin area are described by bounded and continuously differentiable function  $h(y)$ , i.e.

$$\tilde{c}(x) - \tilde{c}(x_0) = h(A(x) - A(x_0)) . \quad (2.21)$$

### 3 Model adaptation

The mathematical model for dissolved oxygen balance (2.16) is involved therefore we simplify it. Consider the river stretch  $[x_0, x]$  we assume the initial condition:

$$k_o(x) \equiv const, \quad k_b(x) \equiv const, \quad k_i(x) \equiv const, \quad k_a(x) \equiv const, \quad v(x) \equiv const, \\ \tilde{c}(x) \equiv const .$$

According to the State Monitoring Programme,  $BDS_5$ ,  $NH_4^+$ ,  $NO_2^-$ ,  $NO_3^-$  and  $O_2$  are measured in five sections P1-P5 of the Neris and four sections Z1-Z4 of Žeimena (Fig. 3.1) once per month. The sewage disposal of the towns Nemenčinė, Pabradė, Švenčionėliai, Jonava and the city of Vilnius is subjected to laboratory monitoring.

We have analysed seven river stretches, namely, P1-P2, P2-P3, P3-P4, P4-P5, and Z1-Z2, Z2-Z3, Z3-Z4. Stretches P1-P2 and Z1-Z2 are the least affected by anthropogenic activity, and for this reason they serve best for the adaptation of a mathematical model and calculation of its coefficients. The mathematical model adapted for the first stretch is then applied to other stretches.

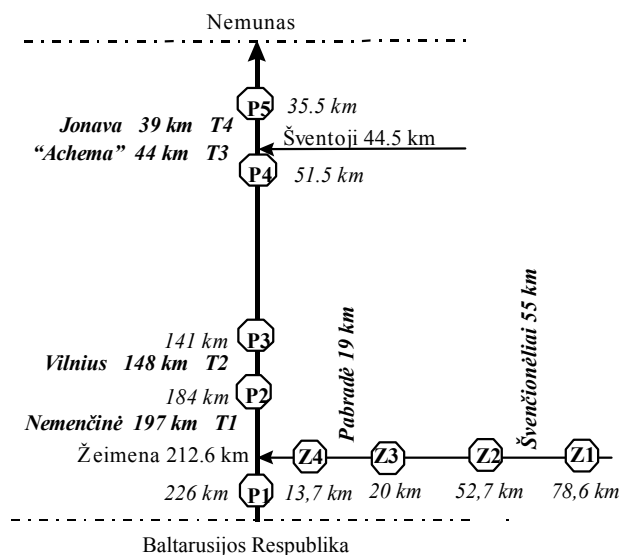


Fig.3.1. State monitoring sections (1996).

Model adaptation is the first stage of testing and tuning a model to a set of field data, preferably a set of field data not used in the original model construction. The distributed source, chemical and biological kinetic coefficients may be determined from statistical analysis.

Adapting water quality model, the analyst selectively determines some model-input parameters that, when used in the model, yield reasonable simulations of observed water quality data. Some of these input parameters, such as  $Q$ ,  $\nu$ ,  $BDS_5$ ,  $NH_4^+$ ,  $NO_2^-$ ,  $NO_3^-$ ,  $O_2$ ,  $Cl$ ,  $T$  and solar energy are directly measured. Other model parameters, such as oxidation rates, reaeration rates, nitrification rates, SOD, distributed source, distributed flow, and algae are not directly measured. These parameters are determined by empirical formulas and their values are obtained in the process of model adaptation. The decomposition rate coefficient, reaeration rates coefficients, distributed flow, SOD and algae are determined from empirical formulas. The distributed sources concentration and oxidation rates coefficients are determined by model adaptation (i.e. in terms of the least square deviation)

$$\sum_{i=1}^N (c(t_i) - \tilde{c}(t_i))^2 \longrightarrow \min_{\tilde{c}, k_a, k_i}, \quad (3.1)$$

where  $c(t_i)$  is the measured concentration and  $\tilde{c}(t_i)$  is the value obtained from the model, both at time  $t_i$ .

Goodness of fit of the model and the field data are measured by the correlation coefficient

$$r = \frac{\sum_{i=1}^N (c(t_i) - \bar{c})(\tilde{c}(t_i) - \bar{\tilde{c}})}{\sqrt{\sum_{i=1}^N (\tilde{c}(t_i) - \bar{\tilde{c}})^2 \sum_{i=1}^N (c(t_i) - \bar{c})^2}} \quad (3.2)$$

and the determination coefficient

$$R^2 = 1 - \frac{\sum_{i=1}^N (c(t_i) - \tilde{c}(t_i))^2}{\sum_{i=1}^N (c(t_i))^2} \quad (3.3)$$

where  $\bar{c} = \frac{1}{N} \sum_{i=1}^N c(t_i)$  and  $\bar{\tilde{c}} = \frac{1}{N} \sum_{i=1}^N \tilde{c}(t_i)$ .

On the basis of long-term hydrological and hydrochemical state monitoring data for the Neris River and the Žeimena River, the dependence of dissolved oxygen on the biochemical oxygen demand, nitrification, reaeration, sedimentation, photosynthesis and algae respiration are studied.

Modelling the stretch P1-P2 and assessing the Žeimena River and the town of Nemenčine, we obtain that the  $\text{NH}_4^+$  correlation coefficient  $r$  is 0,98;  $\text{NO}_2^-$  - 0,98;  $\text{NO}_3^-$  - 0,95;  $\text{BDS}_5$  - 0,94 and  $\text{O}_2$  - 0,74 (table 3.1).

When data from a winter survey are first used to calibrate a model, the dissolved oxygen balance is not sensitive to the nitrification rate and, therefore, decomposition rate and distributed source can be determined more accurately. During model validation, another set of data collected in the summer months is used. Since the nitrification process is highly sensitive to the temperature, the modelling analysis is able to tune the nitrification rate with greater accuracy. Then, in winter months error of estimate is smaller than in summer months.

Without assessing the  $\text{BDS}_5$  distributed sources, we obtain that the  $\text{BDS}_5$  determination coefficient is 1,14 time smaller than for simulation through the assessment of distributed sources [11]. The  $\text{NH}_4^+$  determination coefficient is 1,18 ( $\text{NO}_2^-$  gives 1,22,  $\text{NO}_3^-$  gives 1,07) time smaller than for simulation through the assessment of distributed sources and algae quantity [12].

Recall that for the stretch immediately below the discharge, biological activity is primarily heterotrophic. That is, it is dominated by organisms such as bacteria that obtain their energy by consuming organic matter, and in the process, deplete oxygen. Plant growth in this area is suppressed because of a number of factors, including light extinction due to turbidity.

Further downstream, as the stream begins to recover, levels of nutrients such as organic matter (nitrogen, phosphorus) will be high.

Because photosynthesis is light dependent, this effect can have seasonality.

The month average oxygen production due to photosynthesis and reduction due to respiration is formulated as follows:

$$A_0(t+1) - A_0(t) = \frac{c_{o0}(t+1) - c_{o0}(t)}{\beta_1\mu - \beta_2\rho}, \quad t = 1, \dots, 12, \quad (3.4)$$

where  $c_{o0}(t)$  is the dissolved oxygen concentration,  $A$  is the algal biomass concentration,  $\mu$  is the algae growth rate coefficient,  $\rho$  is the algae respiration rate coefficient,  $\beta_1$  is the oxygen production in photosynthesis per unit of algal biomass and  $\beta_2$  is the oxygen uptake in respiration per unit of algal biomass.

Using formula (3.4), the algal biomass concentration in May-October month has been assessed. The largest algal biomass concentration was in spring, and the next largest concentration in autumn (see fig. 3.2). In other months (winter months) the algal biomass concentration was not assessed since the

water temperature and light energy was lower, which means that algal biomass grows slowly or even does not grow at all.

There are two peaks in figure 3.2. In winter months algal biomass growth is slow, since water temperature and light intensity is low, but there is a large amount of accumulated organic matter in the water. Water temperature and light intensity determine the fast algal biomass growth, because biogenic matter (spring flowering) does not limit them. The fast decrease of organic matters, determine the end of flowering and accumulation of organic matter in the water. Then the algal biomass grows fast, i.e. the autumn flowering will continue while the limit factor of algal biomass growth appears (lower water temperature and light intensity).

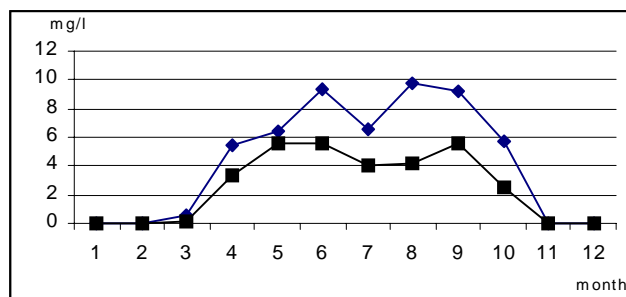


Fig.3.2. Mean algae concentrations in the section P2 1991-1997 m.  
(♦ - section P1; ■ - section Z1)

The simulation of  $O_2$ , without nitrification, algal respiration and photosynthesis assessment, we obtain 1,13 times smaller correlation coefficient. In particular, the process of nitrification as well as the algal affects dissolved oxygen during the warmer period, i.e. without assessing nitrification and algae we have 1,45 times smaller correlation coefficient in May - August.

The  $NH_4^+$ ,  $NO_3^-$  and  $BDS_5$  distributed pollution source has been calculated according to pollution mass balance formula (2.12) in the stretch P1-P2. The largest load of the distributed  $NH_4^+$  ( $NO_3^-$  and  $BDS_5$ ) source is in March-May. The  $NH_4^+$  distributed source is 0,74 and 0,63 kgN/ha month ( $NO_3^-$  - 3,17 and 2,52kgN/ha month,  $BDS_5$  - 59 and 51 kg $O_2$ /ha in month). The smallest load is in July-August ( $NH_4^+$  - 0,15 kgN/ha month;  $NO_3^-$  - 0,47 kgN/ha month;  $BDS_5$  - 26 and 32 kg $O_2$ /ha month) (Fig. 3.3). The yearly load of the distributed  $NH_4^+$  source is 4,3 kgN/ha year,  $NO_3^-$  - 17 kgN/ha year and  $BDS_5$  - 424 kg $O_2$ /ha year.

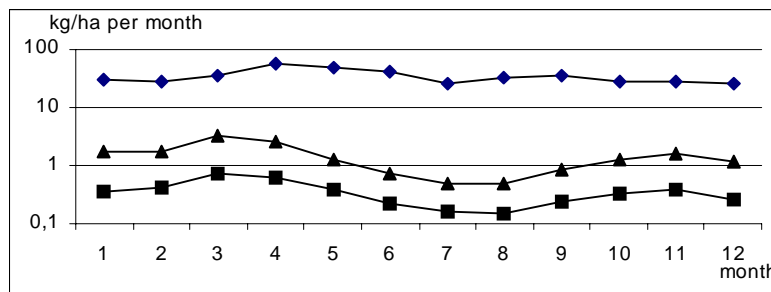


Fig.3.3. The load of the distributed pollution source (NH<sub>4</sub><sup>+</sup>, NO<sub>3</sub><sup>-</sup> and BDS<sub>5</sub>) in the stretch P1-P2 in 1980-1997. (■ - NH<sub>4</sub><sup>+</sup>; ◆ - BDS<sub>5</sub>; ▲ - NO<sub>3</sub><sup>-</sup>)

It has been noted that the distributed sources polluting the Neris depend on the temperature (see fig.3.3). This kind of dependence can be expressed as a regressive equation:

$$\begin{aligned} \tilde{c}_b &= 2,4106T + 12,779; r - 0,91, N - 191, \\ \tilde{c}_a &= 0,0838T + 0,7883; r - 0,92, N - 112, \\ \tilde{c}_e &= -0,2436T + 7,8908; r - 0,93, N - 105. \end{aligned} \quad (3.5)$$

Here  $r$  is the correlation coefficient (equation 3.2) and  $N$  is the number of observation.

The equation (3.5) is reflected the general distributed sources tendency in the stretch P1-P2.

Examining the point source impact (Vilnius City) on the Neris water quality, we use the laboratory monitoring data: the flow of the city of Vilnius and NO<sub>2</sub><sup>-</sup>, NH<sub>4</sub><sup>+</sup>, NO<sub>3</sub><sup>-</sup>, BDS<sub>5</sub> concentrations.

Applying the 1986-1997 model for the stretch P2-P3, we obtain the determination coefficient  $R^2$ : BDS<sub>5</sub> – 0,37 ( $r=0,61$ ) and O<sub>2</sub> – 0,38 ( $r=0,62$ ). Applying the 1991-1997 model for the stretch P2-P3, we obtain the determination coefficient  $R^2$ : NH<sub>4</sub><sup>+</sup> – 0,18 ( $r=0,41$ ) and NO<sub>3</sub><sup>-</sup> – 0,50 ( $r=0,71$ ). Correlation coefficient  $r$  in the section P3 is 1,2-2,4 time smaller than in the section P2.

When modelling stretch P3-P4, it was noted that the sectional measurements are asynchronous. We assume that distributed sources are identical to those in stretch P1-P2. When simulating section P4, we obtain the following correlation coefficient  $r$  is  $\approx 1,2$  time smaller than in the section P2 (see table 3.1). The nitrite concentrations are close to measurement errors.

The simulation errors in the section P4 are greatly affected by the asynchronous nature of measurements between sections P3 and P4. In sections P3 and P4 measurements are taken with a difference of 4 to 15 solar days,

which accounts for the fact that the monitoring data mayn't reflect actual dynamics (i.e. they mayn't reflect actual organic pollution dependence between the sections). It is only with the change of the state monitoring system that the parameters could be assessed with a sufficient degree of accuracy (i.e. in respect to distance and flow rate, measurements in the section P4 should be taken after one to three solar days compared to those in the section P3).

Applying the model for section P5 of the years 1991-1997 in pollution load assessment for the town of Jonava and for "ACHEMA" company, we obtain the correlation coefficient  $r$  in the section P5 is  $\approx 1,6$  time smaller than in the section P2 (see table 3.1).

When modelling the Žeimena River, we obtain the average determination coefficient  $R^2$  in the sections Z2-Z4 is  $\text{NH}_4^+$  - 0,86;  $\text{NO}_3^-$  - 0,83;  $\text{BDS}_5$  - 0,72 and  $\text{O}_2$  - 0,68 (Table 3.1). The nitrite concentrations are close to measurement errors.

**Table 3.1. The results of statistical assessment of the mathematical model of the Neris and the Žeimena.**

Section	$\text{BDS}_5$		$\text{O}_2$		$\text{NH}_4^+$		$\text{NO}_2^-$		$\text{NO}_3^-$	
	$r$	$R^2$	$r$	$R^2$	$r$	$R^2$	$r$	$R^2$	$r$	$R^2$
P2	0,94	0,88	0,74	0,55	0,98	0,96	0,98	0,96	0,95	0,90
P3	0,61	0,38	0,64	0,47	0,53	0,28			0,70	0,49
P4	0,75	0,56	0,62	0,38	0,93	0,86			0,77	0,59
P5	0,52	0,27			0,56	0,31			0,68	0,46
Z2	0,89	0,79	0,80	0,64	0,91	0,83			0,91	0,83
Z3	0,81	0,66	0,73	0,53	0,93	0,87			0,94	0,88
Z4	0,85	0,72	0,93	0,86	0,94	0,88			0,88	0,77

The smaller load of the distributed  $\text{NH}_4^+$  ( $\text{NO}_3^-$  and  $\text{BDS}_5$ ) source is 4,5 kgN/ha year ( $\text{NO}_3^-$  - 1,45 kgN/ha year,  $\text{BDS}_5$  - 21 kgO<sub>2</sub>/ha year) in the stretch Z1-Z2. The load of the distributed  $\text{NH}_4^+$  ( $\text{NO}_3^-$  and  $\text{BDS}_5$ ) source in the stretch Z2-Z3 is 2-4 time larger than in the stretch Z1-Z2.

In comparing the distributed sources in Žeimena and Neris Rivers, it was noticed that in the similar area of used land (40% agricultural land, 52% - forest and 3% water (calculated using programs "ArcView" and "Corine")) distributed source of  $\text{BDS}_5$  in the stretch P1-P2 of Neris River, increased twice the pollution in the stretch Z3-Z4 of Žeimena River caused by anthropogenical impact. Besides, there are the same seasonal prevalence of distributed source in Žeimena and Neris Rivers, i.e. there is increasing in spring, decreasing in summer, in the other seasons the pollution is constant.

Using the state monitoring data for sections P2 and P3, one can estimate the  $\text{NO}_2^-$ ,  $\text{NH}_4^+$ ,  $\text{NO}_3^-$  and  $\text{BDS}_5$  pollution load of the Vilnius city. Using the

equation (2.12), we obtain

$$\tilde{c} = \frac{c(x_0+) (Q(x_0-) + \tilde{Q}) - c(x_0-) Q(x_0-)}{\tilde{Q}} \quad (3.6)$$

where  $\tilde{Q}$  and  $\tilde{c}$  are the point flow and  $BDS_5$  ( $NH_4^+$ ,  $NO_2^-$ ,  $NO_3^-$ ) concentration, while  $Q(x_0-)$ ,  $c(x_0-)$  and  $c(x_0+)$  stand for the river flow,  $BDS_5$  ( $NH_4^+$ ,  $NO_2^-$ ,  $NO_3^-$ ) concentration before the confluence and after it.

The calculated  $NO_2^-$  and  $NH_4^+$  pollution loads for 1980-1997 differ about 15%,  $NO_3^-$  about 26% and  $BDS_5$  about 18% from the Vilnius sewage disposal laboratory monitoring data (Fig.3.4) [11, 12].

$NH_4^+$  and  $NO_2^-$  oxidation rate coefficients ( $k_a$  and  $k_i$ ) before and after the purification plants of the city of Vilnius were fluctuating in the range 0,04-0,29 and 0,1-0,65, 0,84-2,86 and 0,48-1,7  $d^{-1}$ .

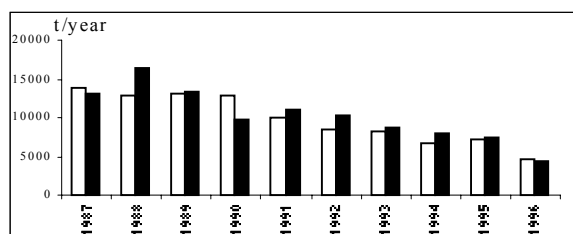


Fig.3.4. Estimated  $BDS_5$  pollution load brought from the Vilnius city purification plants in the years 1987-1996.

( - data from the Sewage Laboratory of Vilnius city. ■ - model estimates based on the monitoring data in sections P2 and P3)

Using the state monitoring data for sections P4 and P5, may be estimate the  $NO_2^-$ ,  $NH_4^+$ ,  $NO_3^-$  and  $BDS_5$  pollution load of the Jonava city and the "ACHEMA" company.

#### 4 Time series analysis

In order to establish the long-term tendencies of the water quality parameters, i.e. the concentrations of  $BDS_5$ ,  $NO_3^-$ ,  $NH_4^+$  and  $O_2$ , we apply the standard time series model

$$X_t = m_t + S_t + Y_t, \quad t = 1, \dots, N. \quad (4.1)$$

Here  $m_t$  is a deterministic trend,  $S_t$  is a deterministic seasonal component with the natural period  $T$  of 12 months ( $T=12$ ,  $S_t = S_{t+T}$  and

$\sum_{j=1}^T S_{j+t} = 0, \forall t$ ),  $Y_t$  is a random component, and  $N$  is the number of observations.

When analysing the time series of  $\text{NH}_4^+$  in the Neris River, we replace  $X_t$  in (4.1) by

$$Z_t = \ln(X_t). \quad (4.2)$$

Since  $N$  the number of observations of the time series analysed, is comparatively small, it is reasonable to use trend models containing only a few parameters to be identified. We apply a linear model for the trend, i.e.

$$m_t = a + bt, \quad (4.3)$$

where  $a$  and  $b$  are unknown coefficients.

The coefficients of deterministic components ( $m_t$  and  $S_t$ ) are estimated by the Ordinary Least-Squares method (OLS).

Denote by  $\hat{m}_t$  and  $\hat{S}_t$  the estimated trend and seasonal components. For the series:

$$\hat{Y}_t = X_t - \hat{m}_t - \hat{S}_t, \quad (4.4)$$

we apply the autoregressive moving average (ARMA) model:

$$\hat{Y}_t + \sum_{i=1}^p c_i \hat{Y}_{t-i} = \varepsilon_t + \sum_{j=1}^q d_j \varepsilon_{t-j}, t = 0, 1, \dots, N, \quad (4.5)$$

where  $\varepsilon_t$  is a white noise series.

The coefficients  $c_i$  and  $d_j$  are estimated using the OLS method (statistical package STATISTICA 5.0).

The  $p$ -value is used in the package to evaluate the null hypothesis validity.

Recall that the  $p$ -value is the probability that the  $t$ -statistic (in the case, when  $H_0$  is true) is not less than the observed value of the  $t$ -statistic.

Let  $\alpha$  denote a *significance level* and  $p$  denote a  $p$ -value. The hypothesis  $H_0$  is accepted if  $p \geq \alpha$ , and is rejected otherwise.

For testing the null hypothesis  $b = 0$  ( $H_0: b = 0$ ) against the alternative  $b \neq 0$  ( $H_1: b \neq 0$ ) we use  $t$ -statistic and standard significance level  $\alpha = 0,05$ . For the BDS<sub>5</sub>, we obtain that the null hypothesis is accepted ( $p$ -value is  $0,3 \div 0,9$ ).

The parameter  $a$  is estimated by  $\hat{a} = \frac{1}{N} \sum_{t=1}^N X_t$ .

By  $N$  we denote the number of complete periods, so that  $a = 1, \dots, n$ . Given this notation, a sequence  $X_t$  ( $t = 1, \dots, N$ ) can be written as  $X_{i+pa}$  ( $i = 1, \dots, p$ ,  $a = 1, \dots, n$ ).

The seasonal coefficients  $\hat{s}_i$  of  $\hat{S}_t$  are calculated as follows:

$$\hat{s}_i = \frac{1}{n} \sum_{a=1}^n (X_{i+pa} - \hat{m}_{i+pa}). \quad (4.6)$$

In fig. 4.1, the BDS<sub>5</sub> time series seasonal coefficients  $\hat{s}_i$  in the Neris and the Žeimena are plotted. Statistical analysis shows that the seasonal coefficients  $s_{12}(P3)$ ,  $s_9(P4)$ ,  $s_7(Z1)$ ,  $s_{12}(Z1)$ ,  $s_2(Z2)$ ,  $s_7(Z2)$ ,  $s_7(Z3)$ ,  $s_2(Z4)$ ,  $s_5(Z4)$ ,  $s_6(Z4)$ ,  $s_7(Z4)$ ,  $s_{10}(Z4)$ , and  $s_{11}(Z4)$  are statistically insignificant at the 0,05 significance level ( $p$ -values are 0,42, 0,31, 0,85, 0,69, 0,65, 0,48, 0,12, 0,12, 0,15, 0,9, 0,64, 0,6, and 0,45, respectively). The remaining seasonal coefficients are statistically significant at the 0,05 significance level.

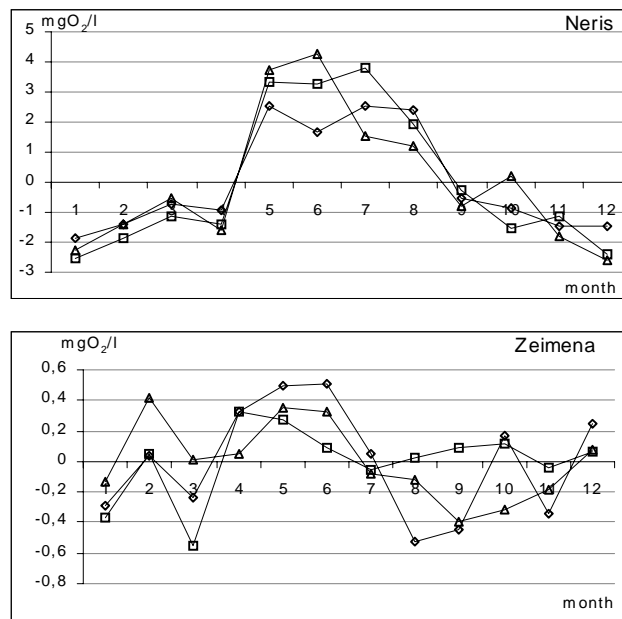


Fig.4.1. The seasonal coefficients  $\hat{s}_i$ . ( $\diamond$  in the sections P1, P2, Z1 and Z2;  $\Delta$  in the sections P3 and Z3;  $\square$  in the sections P4, P5 and Z4, respectively)

In order to test hypothesis about ARMA coefficients significantly analysis of ARMA coefficients, we assume that the series  $\hat{Y}_t$  is Gaussian.

For the series  $\hat{Y}_t$ , we can define its autocorrelation function is defined by:

$$R_{\hat{Y}}(s) = E\hat{Y}(t)\hat{Y}(t+s), \quad \forall t. \quad (4.7)$$

It's necessary to emphasize, that *p-values* are calculated according to supposition, that  $\hat{Y}_t$  is white Gaussian noise, wich isn't correct, as it shows further statistical analysis.

Statistical analysis of series  $\hat{Y}_t$  shows that  $R_{\hat{Y}}$  has a positive peak at lag 1, i.e.  $R_{\hat{Y}}(1)$  is 0,2 in section P1, 0,19 in section P2, 0,27 in section P3, 0,45 in section P4, and 0,26 in section P5 and all them are non zero with the significance level  $\alpha=0,05$  (N=96). For the Žeimena, the  $R_{\hat{Y}}(1)$  in all sections assumes small value in a ranging from 0,08 to 0,14 and can be assumed to be zero ( $p=0,3$ ). Thus, for the series  $\hat{Y}_t$  the model is that of AR(1) in the Neris River and a pure white noise in the Žeimena River.

Thus, for the series  $\hat{Y}_t$ , the chosen model is AR(1). For this model the Mean Square Error (MSE) is 3,73 in the section P1, 2,93 in the section P2, 6,06 in the section P3, 4,35 in the section P4 and 2,87 in the section P5.

Finally, the statistical analysis of the residual series  $\hat{\varepsilon}_t$  shows that  $R_{\hat{\varepsilon}}(t)$ ,  $t > 0$ , can be assumed to be zero ( $p = 0,3 \div 0,92$ ). Hence, the series  $\varepsilon_t$  is actually a pure white noise.

Hence, the estimated model for the BDS<sub>s</sub> can be written as:

$$\begin{array}{ll} \text{P1: } \hat{X}_t = 3,31 + \hat{s}_i(\text{P1}) + \hat{Y}_t, & \hat{Y}_t + 0,2\hat{Y}_{t-1} = \hat{\varepsilon}_t, \\ \text{P2: } \hat{X}_t = 3,13 + \hat{s}_i(\text{P2}) + \hat{Y}_t, & \hat{Y}_t + 0,19\hat{Y}_{t-1} = \hat{\varepsilon}_t, \\ \text{P3: } \hat{X}_t = 6,42 + \hat{s}_i(\text{P3}) + \hat{Y}_t, & \hat{Y}_t + 0,27\hat{Y}_{t-1} = \hat{\varepsilon}_t, \\ \text{P4: } \hat{X}_t = 5,26 + \hat{s}_i(\text{P4}) + \hat{Y}_t, & \hat{Y}_t + 0,45\hat{Y}_{t-1} = \hat{\varepsilon}_t, \\ \text{P5: } \hat{X}_t = 4,14 + \hat{s}_i(\text{P5}) + \hat{Y}_t, & \hat{Y}_t + 0,26\hat{Y}_{t-1} = \hat{\varepsilon}_t, \\ \text{Z1: } \hat{X}_t = 1,59 + \hat{s}_i(\text{Z1}) + \hat{Y}_t, & \hat{Y}_t = \varepsilon_t, \\ \text{Z2: } \hat{X}_t = 1,68 + \hat{s}_i(\text{Z2}) + \hat{Y}_t, & \hat{Y}_t = \varepsilon_t, \\ \text{Z3: } \hat{X}_t = 1,6 + \hat{s}_i(\text{Z3}) + \hat{Y}_t, & \hat{Y}_t = \varepsilon_t, \\ \text{Z4: } \hat{X}_t = 1,8 + \hat{s}_i(\text{Z4}) + \hat{Y}_t, & \hat{Y}_t = \varepsilon_t. \end{array} \quad (4.8)$$

The seasonal coefficients  $\hat{s}_i(\text{P1})$ ,  $\hat{s}_i(\text{P2})$ ,  $\hat{s}_i(\text{P3})$ ,  $\hat{s}_i(\text{P4})$ ,  $\hat{s}_i(\text{P5})$ ,  $\hat{s}_i(\text{Z1})$ ,  $\hat{s}_i(\text{Z2})$ ,  $\hat{s}_i(\text{Z3})$  and  $\hat{s}_i(\text{Z4})$  are given in the table 4.1.

Table 4.1. The seasonal coefficients  $\hat{s}_i(\text{P1}) - \hat{s}_i(\text{P5})$  and  $\hat{s}_i(\text{Z1}) - \hat{s}_i(\text{Z4})$ .

Month	I	II	III	IV	V	VI	VII	VIII	IX	X	XI	XII
<b>BDS<sub>5</sub></b>												
$\hat{s}_i(\text{P1})$	-1,86	-1,38	-0,73	-0,90	2,53	1,69	2,54	2,41	-0,54	-0,85	-1,46	-1,45
$\hat{s}_i(\text{P2})$	-1,66	-1,67	-0,98	-0,72	2,65	2,29	2,13	2,27	-0,70	-0,93	-1,20	-1,47
$\hat{s}_i(\text{P3})$	-2,23	-1,42	-0,50	-1,61	3,75	4,30	1,51	1,23	-0,81	0,19	-1,80	-2,61
$\hat{s}_i(\text{P4})$	-2,56	-1,87	-1,16	-1,41	3,30	3,28	3,81	1,96	-0,27	-1,53	-1,15	-2,41
$\hat{s}_i(\text{P5})$	-1,83	-1,21	-0,89	-0,68	1,31	3,48	3,67	2,47	-0,50	-1,96	-1,78	-2,07
$\hat{s}_i(\text{Z1})$	-0,23	0,45	-0,24	0,07	0,81	0,04	0,08	-0,33	-0,29	-0,04	-0,24	-0,08
$\hat{s}_i(\text{Z2})$	-0,29	0,03	-0,24	0,33	0,50	0,51	0,05	-0,53	-0,44	0,17	-0,34	0,25
$\hat{s}_i(\text{Z3})$	-0,13	0,41	0,01	0,05	0,35	0,32	-0,08	-0,12	-0,39	-0,32	-0,18	0,08
$\hat{s}_i(\text{Z4})$	-0,37	0,04	-0,55	0,32	0,27	0,09	-0,05	0,02	0,08	0,12	-0,05	0,07
<b>NO<sub>3</sub><sup>-</sup></b>												
$\hat{s}_i(\text{P1})$	0,42	0,51	0,33	0,34	-0,31	-0,41	-0,40	-0,32	-0,26	-0,15	0,03	0,22
$\hat{s}_i(\text{P2})$	0,48	0,37	0,22	-0,35	-0,48	-0,46	-0,31	-0,13	-0,08	0,14	0,20	0,41
$\hat{s}_i(\text{P3})$	0,37	0,40	0,32	0,30	-0,39	-0,56	-0,45	-0,39	-0,21	-0,07	0,21	0,48
$\hat{s}_i(\text{P4})$	0,67	0,79	0,76	0,24	-0,55	-0,75	-0,63	-0,76	-0,44	0,09	0,15	0,42
$\hat{s}_i(\text{P5})$	0,79	0,81	0,61	0,26	-0,17	-0,55	-0,78	-0,81	-0,62	-0,26	0,17	0,55
$\hat{s}_i(\text{Z1})$	0,05	0,27	0,18	0,13	-0,04	-0,02	-0,17	-0,16	-0,14	-0,14	-0,01	0,05
$\hat{s}_i(\text{Z2})$	0,18	0,26	0,18	0,11	-0,13	-0,10	-0,17	-0,18	-0,14	-0,08	0,00	0,09
$\hat{s}_i(\text{Z3})$	0,15	0,14	0,26	0,08	-0,12	-0,13	-0,23	-0,17	-0,15	-0,07	0,11	0,13
$\hat{s}_i(\text{Z4})$	0,14	0,12	0,18	0,05	-0,14	-0,08	-0,22	-0,15	-0,14	-0,06	0,06	0,24
<b>NH<sub>4</sub><sup>+</sup></b>												
$\hat{s}_i(\text{P1})$	0,28	0,55	0,65	0,14	-0,61	-0,34	-0,87	-0,58	-0,19	0,71	0,04	0,22
$\hat{s}_i(\text{P2})$	0,89	0,72	0,41	0,00	-0,15	-0,25	-0,76	-0,82	-0,56	-0,29	0,17	0,63
$\hat{s}_i(\text{P3})$	0,68	0,76	0,35	0,16	-0,23	-0,55	-0,53	-0,75	-0,37	-0,14	0,19	0,42
$\hat{s}_i(\text{P4})$	0,43	0,26	0,51	-0,06	0,04	-0,29	-0,34	-0,72	-0,55	0,00	0,33	0,39
$\hat{s}_i(\text{P5})$	0,43	0,26	0,51	-0,06	0,04	-0,29	-0,34	-0,72	-0,55	0,00	0,33	0,39
$\hat{s}_i(\text{Z1})$	0,04	0,01	0,01	-0,01	-0,01	0,01	-0,03	-0,01	-0,03	0,01	0,01	0,01
$\hat{s}_i(\text{Z2})$	0,03	0,04	0,01	-0,01	-0,02	-0,02	-0,02	-0,03	-0,02	0,01	0,01	0,04
$\hat{s}_i(\text{Z3})$	0,02	0,04	0,02	-0,01	-0,03	0,00	-0,03	-0,03	-0,02	0,01	0,02	0,03
$\hat{s}_i(\text{Z4})$	0,03	0,05	0,01	-0,01	-0,02	-0,04	-0,02	-0,04	-0,03	0,01	0,02	0,03
<b>O<sub>2</sub></b>												
$\hat{s}_i(\text{Z1})$	0,19	0,09	1,26	1,46	0,43	-0,62	-0,57	-1,17	-0,77	-0,52	-0,18	0,40
$\hat{s}_i(\text{Z2})$	0,27	0,15	1,21	0,90	-0,03	-0,52	-1,01	-0,97	-0,42	-0,04	-0,16	0,62
$\hat{s}_i(\text{Z3})$	0,23	0,03	1,30	0,57	-0,14	-0,51	-1,01	-0,51	-0,34	0,06	-0,10	0,43
$\hat{s}_i(\text{Z4})$	0,23	0,06	1,30	0,35	-0,36	-0,41	-1,34	0,03	-0,20	-0,04	0,01	0,38

The same statistical analysis for the  $\text{NO}_3^-$  shows that the null hypothesis  $H_0: b=0$  is accepted ( $p$ -value is  $0,12 \div 0,82$ ,  $\alpha$  is  $0,05$ ). Thus, the trend is

$$\hat{m}_t = \hat{a} = \frac{1}{N} \sum_{t=1}^N X_t.$$

Fig. 4.2 represents the  $\text{NO}_3^-$  seasonal coefficients  $\hat{s}_i$  in the Neris and the Žeimena. Statistical analysis shows that the seasonal coefficients  $s_{10}(\text{P2})$ ,  $s_{10}(\text{P3})$ ,  $s_{10}(\text{P5})$ ,  $s_4(\text{P4})$ ,  $s_{10}(\text{P4})$ ,  $s_{11}(\text{P4})$ ,  $s_3(\text{Z1})$ ,  $s_4(\text{Z1})$ ,  $s_{10}(\text{Z1})$ ,  $s_9(\text{Z2})$ ,  $s_4(\text{Z4})$ , and  $s_9(\text{Z4})$  are statistically insignificant at the  $0,05$  significance level ( $p$ -values are  $0,38, 0,36, 0,32, 0,47, 0,28, 0,09, 0,63, 0,89, 0,24, 0,78, 0,09$ , and  $0,13$ , respectively). The remaining seasonal coefficients are statistically significant at the  $0,05$  significance level.

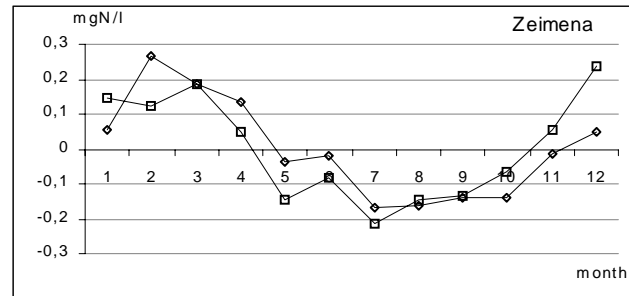


Fig. 4.2. The seasonal coefficients  $\hat{s}_i$ .

( $\diamond$  in the sections P1-P3, Z1 and Z2;  $\square$  in the sections P4, P5, Z3 and Z4, respectively)

After estimation of the components (trend and seasonal), and the computation of the residuals. The series  $\hat{Y}_t$  autocorrelation function  $R_{\hat{Y}}(s)$  showed significant peaks at lags 1 at the  $\alpha=0,05$  in the sections P1-P5 and Z3-Z4. The  $R_{\hat{Y}}(s)$  in the sections Z1-Z2 reveals a pure white noise.

For the series  $\hat{Y}_t$  the model  $\text{AR}(1)$  can be chosen. For this model the  $MSE$  are  $0,049$  in the section P1,  $0,054$  in the section P2,  $0,04$  in the section P3,  $0,17$  in the section P4,  $0,2$  in the section P5,  $0,028$  in the section Z3 and  $0,023$  in the section Z4. The statistical analysis of the residual series  $\hat{\varepsilon}_t$  shows that  $R_{\hat{\varepsilon}}(t) = 0$ ,  $t > 0$ , ( $p = 0,73 \div 0,87$ ). Thus, the series  $\varepsilon_t$  is actually a pure white noise. Hence, the estimated model for the  $\text{NO}_3^-$  can be written as:

$$\begin{aligned} \text{P1: } \hat{X}_t &= 0,68 + \hat{s}_t(\text{P1}) + \hat{Y}_t, & \hat{Y}_t + 0,46\hat{Y}_{t-1} &= \hat{\varepsilon}_t, \\ \text{P2: } \hat{X}_t &= 0,69 + \hat{s}_t(\text{P2}) + \hat{Y}_t, & \hat{Y}_t + 0,36\hat{Y}_{t-1} &= \hat{\varepsilon}_t, \end{aligned} \quad (4.9)$$

$$\begin{array}{ll}
\text{P3: } \hat{X}_t = 0,79 + \hat{s}_i(\text{P3}) + \hat{Y}_t, & \hat{Y}_t + 0,23\hat{Y}_{t-1} = \hat{\varepsilon}_t, \\
\text{P4: } \hat{X}_t = 0,94 + \hat{s}_i(\text{P4}) + \hat{Y}_t, & \hat{Y}_t + 0,54\hat{Y}_{t-1} = \hat{\varepsilon}_t, \\
\text{P5: } \hat{X}_t = 1,04 + \hat{s}_i(\text{P5}) + \hat{Y}_t, & \hat{Y}_t + 0,53\hat{Y}_{t-1} = \hat{\varepsilon}_t, \\
\text{Z1: } \hat{X}_t = 0,38 + \hat{s}_i(\text{Z1}) + \hat{Y}_t, & \hat{Y}_t = \varepsilon_t, \\
\text{Z2: } \hat{X}_t = 0,42 + \hat{s}_i(\text{Z2}) + \hat{Y}_t, & \hat{Y}_t = \varepsilon_t, \\
\text{Z3: } \hat{X}_t = 0,47 + \hat{s}_i(\text{Z3}) + \hat{Y}_t, & \hat{Y}_t + 0,23\hat{Y}_{t-1} = \hat{\varepsilon}_t, \\
\text{Z4: } \hat{X}_t = 0,51 + \hat{s}_i(\text{Z4}) + \hat{Y}_t, & \hat{Y}_t + 0,22\hat{Y}_{t-1} = \hat{\varepsilon}_t.
\end{array}$$

The seasonal coefficients  $\hat{s}_i(\text{P1})$ ,  $\hat{s}_i(\text{P2})$ ,  $\hat{s}_i(\text{P3})$ ,  $\hat{s}_i(\text{P4})$ ,  $\hat{s}_i(\text{P5})$ ,  $\hat{s}_i(\text{Z1})$ ,  $\hat{s}_i(\text{Z2})$ ,  $\hat{s}_i(\text{Z3})$  and  $\hat{s}_i(\text{Z4})$  are given in the table 4.1.

When examining the ammonia nitrogen ( $\text{NH}_4^+$ ) time series in the Neris River (sections P1-P5) we observe that it is difficult to separate the seasonal component from the data. Therefore, we first perform the following data transformation. For the Žeimena, the  $\text{NH}_4^+$  time series of sections Z1-Z4 are analysed by equation (4.1).

For the  $\text{NH}_4^+$  we obtain that  $H_0: b=0, c=0$  is rejected in sections P1-P5 and Z4 (the significance level  $\alpha=0,05$  is greater than  $p$ -value of 0,002) and is accepted in sections Z1-Z3 ( $p \geq \alpha$ , i.e.  $p=0,1, \alpha=0,05$ ). Thus, we reject the null hypothesis that the series has a linear trend  $m_t = a + bt$  (P1-P3, Z4) and parabolic trend  $m_t = a + bt + ct^2$  (P4 and P5).

Fig. 4.3 represents the  $\text{NH}_4^+$  time series seasonal coefficients  $\hat{s}_i$  in the Neris and the Žeimena. Statistical analysis shows that the seasonal coefficients for the Neris  $s_4(\text{P1})$ ,  $s_4(\text{P3})$ ,  $s_9(\text{P3})$ ,  $s_{10}(\text{P3})$ ,  $s_{12}(\text{P3})$ ,  $s_9(\text{P4})$ ,  $s_{10}(\text{P4})$ ,  $s_4(\text{P5})$ ,  $s_5(\text{P5})$ , and  $s_{10}(\text{P5})$  are statistically insignificant at the 0,05 significance level ( $p$ -values are 0,6, 0,16, 0,32, 0,83, 0,06, 0,36, 0,99, 0,94, 0,27, and 0,99, respectively). The other seasonal coefficients are statistically significant at the 0,05 significance level. The seasonal coefficients for the Žeimena  $s_2(\text{Z2})$ ,  $s_8(\text{Z2})$ ,  $s_2(\text{Z3})$ ,  $s_2(\text{Z4})$ ,  $s_6(\text{Z4})$ , and  $s_8(\text{Z4})$  are statistically significant ( $p$ -values are 0,02, 0,03, 0,04, 0,04, 0,02, 0,03, and 0,04, respectively), and the other seasonal coefficients are statistically insignificant ( $p$ -value is  $0,07 \div 0,95$ ) at the 0,05 significance level.

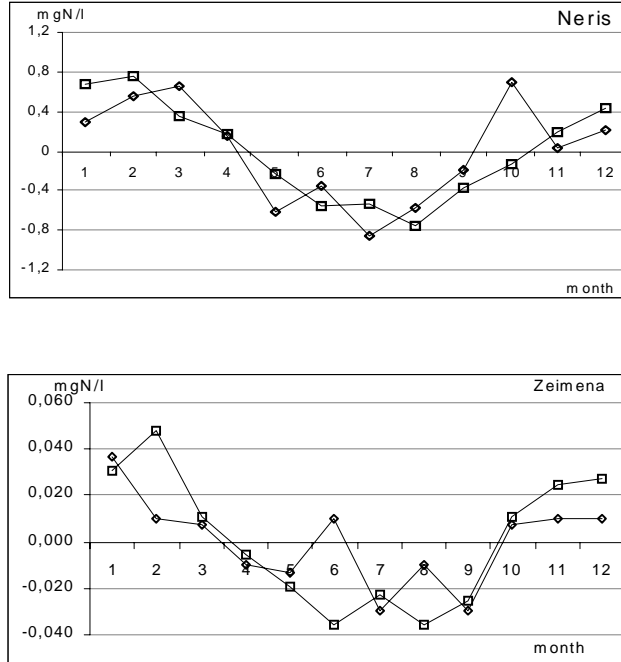


Fig.4.3. The seasonal coefficients  $\hat{s}_i$ .

( $\diamond$  in sections P1 and Z1;  $\square$  in sections P3-P5 and Z2-Z4, respectively)

The  $R_{\hat{Y}}(s)$  has a positive peak at lag 1, i.e.  $R_{\hat{Y}}(1)$  are 0,35 in the section P1, 0,46 in the section P2, 0,51 in the section P3, and 0,43 in the section P5 at the  $\alpha=0,05$  ( $N=96$ ). For the Zeimena, the  $R_{\hat{Y}}(1)$  are 0,43 in the section Z2, 0,36 in the section Z3 and 0,45 in the section Z4, and all them are non zero with  $\alpha=0,05$  ( $N=36$ ). The autocorelation function of  $\hat{Y}_t$  in the sections P4 and Z1 reveals a pure white noise.

For the series  $\hat{Y}_t$  the chosen model is that of AR(1) model, we obtain the MSE: 0,34 in P1, 0,35 in P2, 0,52 in P3, 0,24 in P5 and 0,0004 in Z2-Z4. The statistical analysis of series  $\hat{\varepsilon}_t$  shows that  $R_{\hat{\varepsilon}}(t)$ ,  $t > 0$ , can be assumed to be zero ( $p = 0,3 \div 0,68$ ), i.e.  $\varepsilon_t$  is actually a pure white noise series.

Hence, the estimated model for the  $\text{NH}_4^+$  can be written as:

$$\begin{aligned}
 \text{P1: } \hat{Z}_t &= -1,05 - 0,023t + \hat{s}_i(\text{P1}) + \hat{Y}_t, & \hat{Y}_t + 0,35\hat{Y}_{t-1} &= \hat{\varepsilon}_t, \\
 \text{P2: } \hat{Z}_t &= -1,1 - 0,027t + \hat{s}_i(\text{P2}) + \hat{Y}_t, & \hat{Y}_t + 0,46\hat{Y}_{t-1} &= \hat{\varepsilon}_t, \\
 \text{P3: } \hat{Z}_t &= -0,17 - 0,03t + \hat{s}_i(\text{P3}) + \hat{Y}_t, & \hat{Y}_t + 0,52\hat{Y}_{t-1} &= \hat{\varepsilon}_t,
 \end{aligned} \tag{4.10}$$

$$\begin{aligned}
\text{P4: } \hat{Z}_t &= -2,06 - 0,05t - 0,0006t^2 + \hat{s}_i(\text{P4}) + \hat{Y}_t, & \hat{Y}_t &= \varepsilon_t, \\
\text{P5: } \hat{Z}_t &= -1,77 + 0,03t - 0,0004t^2 + \hat{s}_i(\text{P5}) + \hat{Y}_t, & \hat{Y}_t + 0,45\hat{Y}_{t-1} &= \hat{\varepsilon}_t, \\
\text{Z1: } \hat{X}_t &= 0,05 + \hat{s}_i(\text{Z1}) + \hat{Y}_t, & \hat{Y}_t &= \varepsilon_t, \\
\text{Z2: } \hat{X}_t &= 0,048 + \hat{s}_i(\text{Z2}) + \hat{Y}_t, & \hat{Y}_t + 0,43\hat{Y}_{t-1} &= \hat{\varepsilon}_t, \\
\text{Z3: } \hat{X}_t &= 0,044 + \hat{s}_i(\text{Z3}) + \hat{Y}_t, & \hat{Y}_t + 0,37\hat{Y}_{t-1} &= \hat{\varepsilon}_t, \\
\text{Z4: } \hat{X}_t &= 0,074 - 0,0011t + \hat{s}_i(\text{Z4}) + \hat{Y}_t, & \hat{Y}_t + 0,45\hat{Y}_{t-1} &= \hat{\varepsilon}_t.
\end{aligned}$$

The seasonal coefficients  $\hat{s}_i(\text{P1})$ ,  $\hat{s}_i(\text{P2})$ ,  $\hat{s}_i(\text{P3})$ ,  $\hat{s}_i(\text{P4})$ ,  $\hat{s}_i(\text{P5})$ ,  $\hat{s}_i(\text{Z1})$ ,  $\hat{s}_i(\text{Z2})$ ,  $\hat{s}_i(\text{Z3})$  and  $\hat{s}_i(\text{Z4})$  are given in the table 4.1.

Further, we consider the time series of dissolved oxygen ( $\text{O}_2$ ) in the Neris River. It has been noted that the time series has no seasonal component ( $S_t \equiv 0$ ).

Now, usual  $t$ -statistic for  $H_0: b = 0$  reveals that the null hypothesis can be accepted in sections P3-P5 and Z1-Z4 ( $p$ -value is  $0,14 \div 0,9$ ) and is rejected in sections P1 and P2 ( $p$ -value is  $0,006$ ) at the  $0,05$  significance level. Thus, we have linear trend only in the sections P1 and P2.

Fig. 4.4 represents the  $\text{O}_2$  seasonal coefficients  $\hat{s}_i$  in the Žeimena. Statistical analysis shows that the seasonal coefficients  $s_1(\text{Z1})$ ,  $s_2(\text{Z1})$ ,  $s_{11}(\text{Z1})$ ,  $s_5(\text{Z2})$ ,  $s_{10}(\text{Z2})$ ,  $s_{11}(\text{Z2})$ ,  $s_2(\text{Z3})$ ,  $s_5(\text{Z3})$ ,  $s_{10}(\text{Z3})$ ,  $s_{11}(\text{Z3})$ ,  $s_2(\text{Z4})$ , and  $s_8(\text{Z4}) - s_{11}(\text{Z4})$  are statistically insignificant at the  $0,05$  significance level ( $p$ -values are  $0,06$ ,  $0,28$ ,  $0,55$ ,  $0,93$ ,  $0,64$ ,  $0,82$ ,  $0,28$ ,  $0,25$ ,  $0,95$ ,  $0,86$ ,  $0,22$ ,  $0,84$ ,  $0,06$ ,  $0,67$ , and  $0,28$ , respectively). The remaining seasonal coefficients are statistically significant at the  $0,05$  significance level.

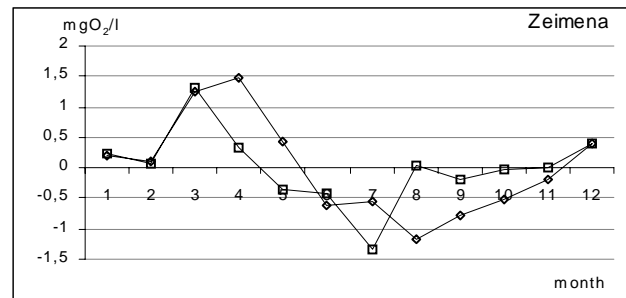


Fig.4.4. The seasonal components  $\hat{s}_i$  in the Žeimena. ( $\diamond$  in the sections Z1 and Z2;  $\square$  in the sections Z3 and Z4)

Comparing of ARMA models, we find that the smallest  $MSE$  are obtained for  $\text{AR}(1)$  models in sections P1, P2 and Z1-Z4 ( $MSE = 2,24$ ,  $2,24$ ,

1,67, 1,55, 1,43 and 1,66, respectively). The best model in the section P3 (P4, P5) is AR(3) (respectively, MA(1), ARMA(1,1)) (MSE are 3,18, 3,35, 2,42). For the Žeimena and the Neris, the autocorrelation function of  $\hat{Y}_t$  is statistically significant by non zero at the 0,05 significance level. Finally, the statistical analysis of the residual series  $\hat{\varepsilon}_t$  shows that  $R_\varepsilon(t) = 0, t > 0$  ( $p = 0,73 \div 0,98$ ). The series  $\varepsilon_t$  is actually a pure white noise. Hence, the estimated model for the O<sub>2</sub> can be written as:

$$\begin{aligned}
 \text{P1: } \hat{X}_t &= 11,29 - 0,02t + \hat{Y}_t, & \hat{Y}_t + 0,39\hat{Y}_{t-1} &= \hat{\varepsilon}_t, & (4.11) \\
 \text{P2: } \hat{X}_t &= 11,32 - 0,02t + \hat{Y}_t, & \hat{Y}_t + 0,56\hat{Y}_{t-1} &= \hat{\varepsilon}_t, \\
 \text{P3: } \hat{X}_t &= 10,04 + \hat{Y}_t, & \hat{Y}_t + 0,36\hat{Y}_{t-1} + 0,18\hat{Y}_{t-2} - 0,16\hat{Y}_{t-3} &= \hat{\varepsilon}_t, \\
 \text{P4: } \hat{X}_t &= 10,83 + \hat{Y}_t, & \hat{Y}_t &= \hat{\varepsilon}_t - 0,07\hat{\varepsilon}_{t-1}, \\
 \text{P5: } \hat{X}_t &= 11,03 + \hat{Y}_t, & \hat{Y}_t + 0,82\hat{Y}_{t-1} &= \hat{\varepsilon}_t + 0,61\hat{\varepsilon}_{t-1}, \\
 \text{Z1: } \hat{X}_t &= 9,56 + \hat{s}_i(\text{Z1}) + \hat{Y}_t, & \hat{Y}_t + 0,37\hat{Y}_{t-1} &= \hat{\varepsilon}_t, \\
 \text{Z2: } \hat{X}_t &= 9,54 + \hat{s}_i(\text{Z2}) + \hat{Y}_t, & \hat{Y}_t + 0,41\hat{Y}_{t-1} &= \hat{\varepsilon}_t, \\
 \text{Z3: } \hat{X}_t &= 9,76 + \hat{s}_i(\text{Z3}) + \hat{Y}_t, & \hat{Y}_t + 0,41\hat{Y}_{t-1} &= \hat{\varepsilon}_t, \\
 \text{Z4: } \hat{X}_t &= 9,76 + \hat{s}_i(\text{Z4}) + \hat{Y}_t, & \hat{Y}_t + 0,34\hat{Y}_{t-1} &= \hat{\varepsilon}_t.
 \end{aligned}$$

The seasonal components  $\hat{s}_i(\text{Z1})$ ,  $\hat{s}_i(\text{Z2})$ ,  $\hat{s}_i(\text{Z3})$  and  $\hat{s}_i(\text{Z4})$  are given in the table 4.1.

The BDS<sub>5</sub>, NO<sub>3</sub><sup>-</sup>, and NH<sub>4</sub><sup>+</sup> time series are analysed similarly to those for the Neris and the Žeimena rivers. The time series for BDS<sub>5</sub>, NO<sub>3</sub><sup>-</sup> and NH<sub>4</sub><sup>+</sup> may be written as a trend  $m_t$ , seasonal component  $S_t$  with the period equal to 12 month, and a random component  $Y_t$ . For the series  $Y_t$ , the best model and the smallest MSE is that of AR(1) model.

## 5 References

1. Steven C. Chapra. *Surface water-quality modelling*. Boston, WCB, 1996
2. D. J. O'Connor, R. V. Thomann, D. M. Di Toro. *Dynamic water quality forecasting and management*. EPA-660/3-73-009. Washington, DC, 1973
3. D. J. O'Connor, R. V. Thomann, D. M. Di Toro. *Analysis of fate of chemicals in receiving waters. Phase 1*. Washington, DC. Prepared by HydroQual instruction, 1981
4. *Technical guidance manual for developing total maximum daily loads. Book 2. Streams and rivers*. Part 1: Biochemical oxygen demand/dissolved oxygen and nutrients/eutrophication. EPA. Washington, DC, 1997

5. *Technical guidance manual for performing waste load allocations. Book 2: Streams and Rivers. Part 1. Biochemical oxygen demand/dissolved oxygen and nutrients/eutrophication.* EPA. Washington, DC, 1997
6. J. A. Muller. *Accuracy of steady-state finite difference solutions.* Hydrosience, 1976
7. R. P. Canale, A. H. Vogel. *Effects of temperature on phytoplakton growth.* Environmental engineering division ASCE 100(EE1), pp. 231-241, 1974
8. *Standard methods for the examination of water and wastewater.* APHA (American Public Health Association).. Washington, DC, 1994
9. R. Daubaras. *Neries baseino upių cheminės sudėties formavimas, hidrocheminė charakteristika ir savaiminis apšvalymas.* Chemijos m. k. disertacija, Vilnius, 1968
10. J. Staniškis, V. Vincevičienė. *Nemuno baseino užterštumo modelio, skirto situacijos kompleksiniam vertinimui ir prognozavimui sukūrimas.* LR Aplinkos ministerija, ataskaita, Vilnius, 1993
11. G. Sakalauskiene. "Vandens organinio užterštumo matematinis modeliavimas Neryje". *Aplinkos Tyrimai, Inžinerija ir Vadyba* v. 9, Nr.2, pp. 19-25, Vilnius, 1999
12. G. Sakalauskiene. "Nitrification in the Neris river (Lithuania)". *Environmental and Chemical Physics* v. 21, № 2. pp. 13-21, Vilnius 1999
13. D. Anderson. *Time series.* Amsterdam, NHPC, 1980
14. *Lietuvos upių vandens kokybės metraštis (1977-1997).* LR Aplinkos ministerija, Vilnius, 1997
15. Н. И. Дружинин, А. И. Шишкин. *Математическое моделирование и прогнозирование загрязнения поверхностных вод суши.* Ленинград, Гидрометеиздат, 1989
16. О. Ф., Васильев Е. В. Еременко. "Моделирование трансформации соединений азота, для управления качеством воды в водотоках". *Водные ресурсы*, № 5. pp. 31-36, 1980
17. А. В. Леонов. *Математическое моделирование трансформации соединений фосфора в пресноводных экосистемах.* Москва, Наука, 1986
18. Г. И. Марчук. *Математическое моделирование в проблеме окружающей среды.* Москва, Наука, 1982
19. И. Г. Журбенко, И. А. Кожевникова. *Стохастическое моделирование процессов.* Москва, Наука, 1990
20. А. И. Шишкин. *Основы математического моделирования конвективного переноса примесей.* Ленинград, ЛТИ, 1976